Structure
Article

Structure and Disassembly of Filaments Formed by the ESCRT-III Subunit Vps24

Sara Ghazi-Tabatabai,[1] Suraj Saksena,[2] Judith M. Short,[1] Ajaybabu V. Pobbati,[1] Dmitry B. Veprintsev,[1] R. Anthony Crowther,[1] Scott D. Emr,[2] Edward H. Egelman,[3] and Roger L. Williams[1,*]
[1]MRC Laboratory of Molecular Biology, Hills Road, Cambridge CB2 0QH, UK
[2]Cornell Institute for Cell and Molecular Biology, Department of Molecular Biology and Genetics, Cornell University, 307 Biotechnology Building, Ithaca, NY 14853, USA
[3]Department of Biochemistry and Molecular Genetics, University of Virginia, Health Sciences Center, Box 800733, Charlottesville, VA 22908-0733, USA
*Correspondence: rlw@mrc-lmb.cam.ac.uk
DOI 10.1016/j.str.2008.06.010

SUMMARY

The ESCRT machinery mediates sorting of ubiquitinated transmembrane proteins to lysosomes via multivesicular bodies (MVBs) and also has roles in cytokinesis and viral budding. The ESCRT-III subunits are metastable monomers that transiently assemble on membranes. However, the nature of these assemblies is unknown. Among the core yeast ESCRT-III subunits, Snf7 and Vps24 spontaneously form ordered polymers in vitro. Single-particle EM reconstruction of helical Vps24 filaments shows both parallel and head-to-head subunit arrangements. Mutations of regions involved in intermolecular assembly in vitro result in cargo-sorting defects in vivo, suggesting that these homopolymers mimic interactions formed by ESCRT-III heteropolymers during MVB biogenesis. The C terminus of Vps24 is at the surface of the filaments and is not required for filament assembly. When this region is replaced by the MIT-interacting motif from the Vps2 subunit of ESCRT-III, the AAA-ATPase Vps4 can both bundle and disassemble the chimeric filaments in a nucleotide-dependent fashion.

INTRODUCTION

Eukaryotic endosomes coordinate the movement of proteins between the plasma membrane, the trans-Golgi network, and the lysosome/vacuole (Katzmann et al., 2002). Proteins that are delivered to the lysosome/vacuole pass through late endosomal structures called multivesicular bodies (MVBs), which consist of a limiting membrane enclosing intralumenal vesicles (ILVs) formed by the invagination of the outer membrane into the lumen (Haigler et al., 1979). Mono-ubiquitination serves as the major entry signal for proteins into the MVB pathway (Katzmann et al., 2001; Piper and Luzio, 2007). Protein sorting into the internal vesicles of MVBs is regulated by the four endosomal sorting complexes required for transport, ESCRT-0, -I, -II, and -III. Mutations in genes encoding ESCRT subunits cause enlarged, "class E," endosomal compartments, and result in sorting defects (Raymond et al., 1992; Odorizzi et al., 1998). ESCRT complexes coordinate the recognition and enrichment of ubiquitinated cargo proteins in regions on endosomal surfaces that bud inward to form ILVs. The AAA-ATPase Vps4 catalyzes the dissociation of the ESCRT machinery from endosomal membranes and is essential for MVB biogenesis and function (Williams and Urbe, 2007; Saksena et al., 2007; Hurley, 2008).

The ESCRT-III complex consists of four core subunits, Vps2/CHMP2, Vps24/CHMP3, Vps20/CHMP6, and Snf7/Vps32/CHMP4 (Babst et al., 2002) and several ESCRT-III-like proteins, such as Did2/CHMP1 and Vps60/CHMP5. All ESCRT-III subunits share a common architecture, with a basic N terminus and an acidic C terminus (Babst et al., 2002). The crystal structure of the core of human CHMP3 consists of an asymmetric four-helical bundle that is likely to be representative of all ESCRT-III subunits (Muziol et al., 2006). These subunits exist as monomers in the cytosol, but form functional lattices of undefined stoichiometry on endosomal membranes (Babst et al., 2002; Bowers et al., 2004). The inactive monomeric form of the subunits is maintained by interactions between the autoinhibitory C terminus and the N-terminal portion of the subunit (Lin et al., 2005; Zamborlini et al., 2006; Muziol et al., 2006; Shim et al., 2007; Lata et al., 2008). How this autoinhibition might be relieved in vivo is unclear, although interactions with other MVB pathway proteins, such as Vps25 (ESCRT-II), and/or membrane binding may account for this. How the ESCRT-III subunits assemble on endosomal membranes is also unclear. Vps20 has a myristoyl group at its N terminus that contributes to membrane binding (Babst et al., 2002; Yorikawa et al., 2005), and the CHMP3 core structure has an extensive, membrane-binding basic surface (Muziol et al., 2006). Human Snf7/CHMP4 binds phosphoinositides in vitro, and when overexpressed in cells forms large polymers on membranes (Lin et al., 2005; Hanson et al., 2008).

The four core ESCRT-III subunits are necessary for cargo sorting in yeast, and deletion of any of these results in class E compartments. ESCRT-0 (Hrs) and ESCRT-I (TSG101) subunits have a role in ILV formation (Razi and Futter, 2006; Lloyd et al., 2002; Doyotte et al., 2005; Rieder et al., 1996; Odorizzi et al., 1998). In contrast, recent studies have shown that CHMP3-depleted cells can form ILVs (Bache et al., 2006), as can cells depleted of ESCRT-III-like subunits CHMP1/Did2 (Nickerson et al., 2006) or CHMP5/Vps60 (Shim et al., 2006), suggesting that ESCRT-III may also have roles in later stages of the pathway.

ESCRT-III subunits recruit the ESCRT-associated protein ALIX (Kim et al., 2005) and the deubiquitinating enzymes UBPY and AMSH to endosomes (Row et al., 2007; Zamborlini et al., 2006; Agromayor and Martin-Serrano, 2006). Recently, non-MVB functions for several ESCRT-III components have been identified (Slagsvold et al., 2006). ESCRT-III has been implicated in the autophagy pathway and in the clearance of protein aggregates that characterize neurodegenerative disorders (Forman et al., 2004; Lee et al., 2007; Filimonenko et al., 2007). Mammalian ESCRT-III also has a role in retroviral budding, as do ESCRT-0, -I, and the ESCRT-associated protein AIP/ALIX (Martin-Serrano et al., 2003; von Schwedler et al., 2003). ESCRT-III components have also been shown to concentrate at the midbody during cell abscission in cytokinesis (Morita et al., 2007; Carlton and Martin-Serrano, 2007), a process that is topologically similar to retroviral budding and ILV formation.

The C termini of the ESCRT-III proteins Vps2 and Did2 contain a consensus sequence (D/E)xxLxxRLxxL(K/R) that is recognized by the N-terminal microtubule-interacting and transport (MIT) domain of Vps4, the AAA-ATPase responsible for disassembling ESCRT complexes from the endosomal membrane (Obita et al., 2007; Stuchell-Brereton et al., 2007; Vajjhala et al., 2007; Nickerson et al., 2006). Like other AAA-ATPases, Vps4 functions as an oligomer. Upon ATP binding, Vps4 may form a dodecamer or tetradecamer, consisting of two stacked rings (Yu et al., 2008; Hartmann et al., 2008). The double ring structure of Vps4 is greatly stabilized via an interaction with the Vta1/LIP5 protein (Azmi et al., 2006; Fujita et al., 2004; Lottridge et al., 2006; Scott et al., 2005; Ward et al., 2005) that also has a MIT domain capable of selectively recruiting some ESCRT-III subunits (Azmi et al., 2008; Xiao et al., 2008).

We find that recombinant ESCRT-III subunits form lattices in vitro. Using electron microscopy (EM), we have determined the 25 Å resolution structure of helical filaments of yeast Vps24 (ScVps24). Mutations of residues forming contacts in these filaments prevent filament formation in vitro and cause cargo-sorting defects in vivo, suggesting that these homopolymers may mimic heteropolymers formed in cells. Vps4 induces both curved bundling and disassembly of chimeric ESCRT-III subunits that were designed to simultaneously form lattices and interact with Vps4. Disassembly of the protein lattices requires both ATPase activity and the MIT domain of the Vps4.

RESULTS

ESCRT-III Proteins Form Lattices In Vitro

The majority of purified recombinant full-length yeast Vps24 (ScVps24) (residues 1–224) elutes on gel filtration at a volume consistent with a monomer or a dimer. However, when this material is concentrated to 10 mg/ml, nearly half of it appears to be polymeric, as it can be readily pelleted in high-speed centrifugation (see Figure S4 available online). EM analysis of ScVps24 solutions concentrated in gel-filtration buffer (20 mM Tris [pH 8.0], 100 mM NaCl) shows that this material forms extensive helical filaments (Figure 1A). These filaments persist even if the material is subsequently diluted in gel-filtration buffer to 0.07 mg/ml (2.5 μM). The negatively stained filaments are heterogeneous in length (80–2000 nm) with a relatively homogeneous diameter (~15 nm) and can twist extensively along their length. Wider filaments that were shorter and more rigid were also observed, although these were rare (Figure 1A, inset ii). Analytical equilibrium ultracentrifugation shows that the recombinant nonpolymeric fraction of Vps24 (i.e., the fraction that is not immediately pelleted) exists as monomers in solution (data not shown). In contrast to ScVps24, human Vps24/CHMP3 did not form filaments. Among the other yeast ESCRT-III proteins (Vps2, Snf7, and Vps20), only Snf7 forms homopolymers in gel-filtration buffer in vitro. Snf7 polymers are extensive and organized into large sheets, rings, and filaments (Figures 1B–1D). However, due to their irregular character, the ScSnf7 polymers have not yet been amenable to structural characterization.

Single-Particle Helical Reconstruction of ScVps24 Filaments

Initial attempts to characterize ScVps24 filaments with Fourier-Bessel methods revealed the most common filaments to be two-stranded, helical structures, whereas less abundant, wider filaments were three-stranded helices (Figure 1A). Even wider filaments, perhaps representing higher-order helices, were also observed, but were too rare for effective characterization. Our structural characterization focused on the two-stranded filaments due to their abundance. Analysis of a total of ~85,000 overlapping segments of two-stranded ScVps24 filaments revealed a highly variable pitch, ranging from 240 to 350 Å, consistent with their flexibility (see Movie S1). Due to the heterogeneity of the data, traditional methods would tend to average these states together (DeRosier and Klug, 1968). Therefore, we used the iterative helical real-space reconstruction (IHRSR) approach for further structural characterization (Egelman, 2000). In order to get homogeneous data sets suitable for single-particle analysis, the segments of the two-stranded filaments were sorted by pitch, based on their crosscorrelations with projections from 12 reference volumes (Figure S1). Based on their diffraction quality, six subsets (260, 270, 280, 290, 300, and 310 Å) were chosen from which independent IHRSR reconstructions were generated. The most populated pitch subsets were 270 and 280 Å, although there was still significant heterogeneity even within these. Further sorting was ruled out, as a balance between homogeneity and the number of segments per subset had to be maintained. The reconstructions did not differ significantly as a function of pitch. The 260 Å pitch subset reconstruction is shown in Figure 2, because this subset gave the best diffraction, with a resolution of 25 Å (Yang et al., 2003). For the more rigid, three-stranded filaments, a reconstruction was generated from ~900 segments, although due to the small data set the stability of this solution is not comparable to the two-stranded data and we cannot be confident of the resolution beyond ~35 Å (data not shown).

The helical reconstructions revealed a characteristically smooth surface running down the length of the filament, with large caps or "knuckles" on the outer surface (Figure 2A). The high-resolution crystal structure of the core of human Vps24 (CHMP3) (Muziol et al., 2006) was used as a model for ScVps24 during manual fitting into both the two- and three-stranded reconstructions. The core of the Vps24 subunit (residues 9–183 from the 222 residue full-length subunit) is an asymmetric four-helix bundle, consisting of a long helical hairpin formed by helices α1 and α2 packed against a shorter helical hairpin, made up of helices α3 and α4. Although residues 9–183 of human

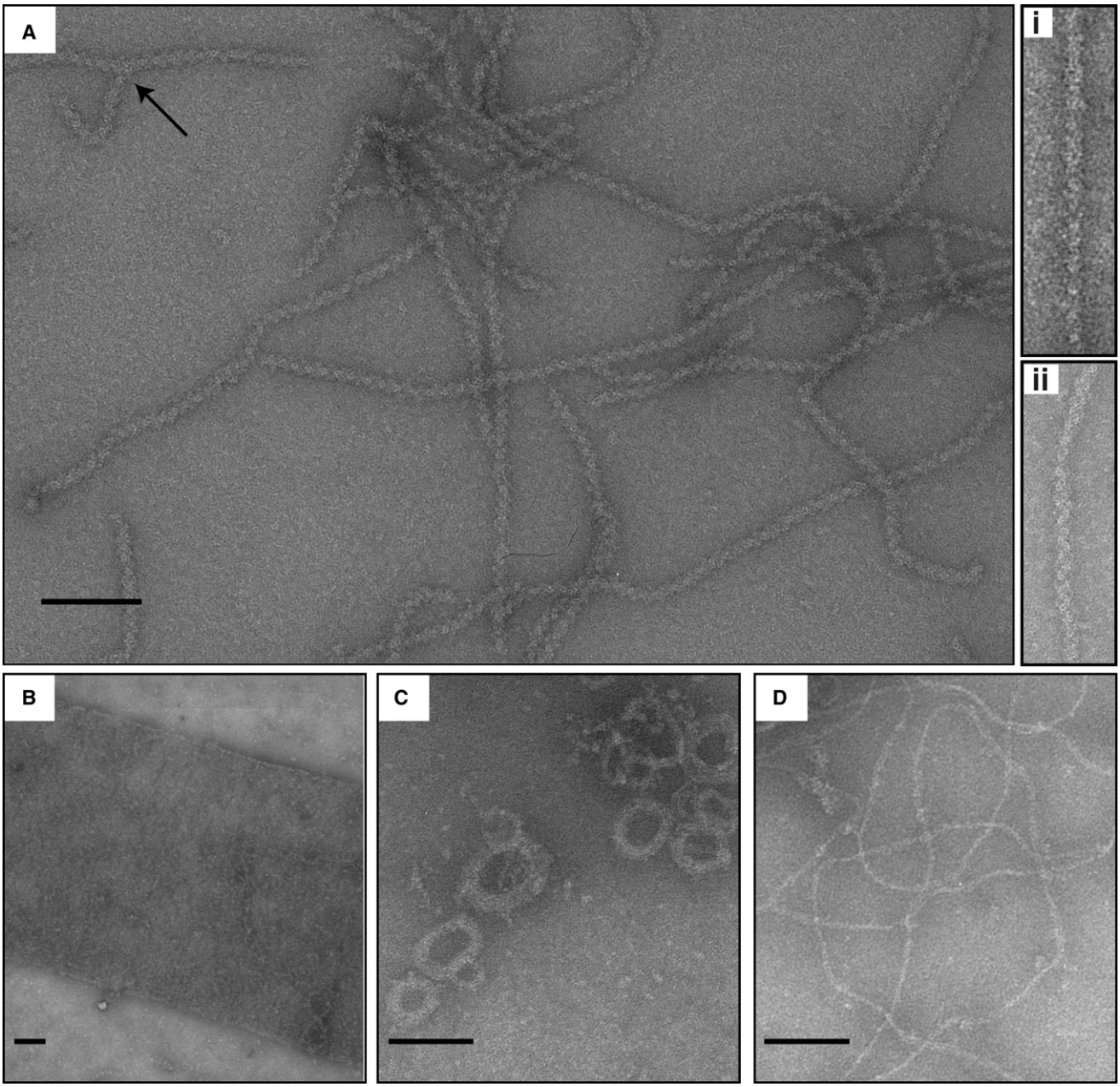

Figure 1. Assemblies Formed by ESCRT-III Subunits In Vitro

(A) Electron micrographs of negatively stained helical filaments of recombinant ScVps24. The arrow points to a branched filament. Inset (i) shows a two-stranded ScVps24 filament (~15 nm diameter) and inset (ii) shows a thicker, three-stranded filament form (~20 nm diameter).

(B–D) Recombinant Snf7 forms sheets (B), rings (C), and strings (D).

The scale bars represent 100 nm.

Vps24 form antiparallel dimers in the crystal structure, and crosslinking suggests that a further truncated form of the subunit (9–163) can form dimers in solution, both full-length and 9–183 human Vps24 are monomeric in solution (Muziol et al., 2006). Furthermore, yeast Vps24 is also a monomer in solution. Extensive efforts to manually fit the dimeric unit seen in the crystal structure of human Vps24 into the reconstructed helical volume were unsuccessful. However, we could readily model single Vps24 subunits into the helical reconstruction. We modeled the ScVps24 filaments with molecules having their longest axis running along the smooth surface of the filament at an angle of ~60° with respect to the z axis. The loop of the α1/α2 helical hairpin points toward the center of the filament, and the C terminus (equivalent to residues 184–222 of human Vps24, which are not present in the crystal structure) radiates outward, with the C termini of two Vps24 molecules from one strand contributing to the density of each knuckle (Figure 2C). However, the C-terminal region is not necessary for filament formation, because purified

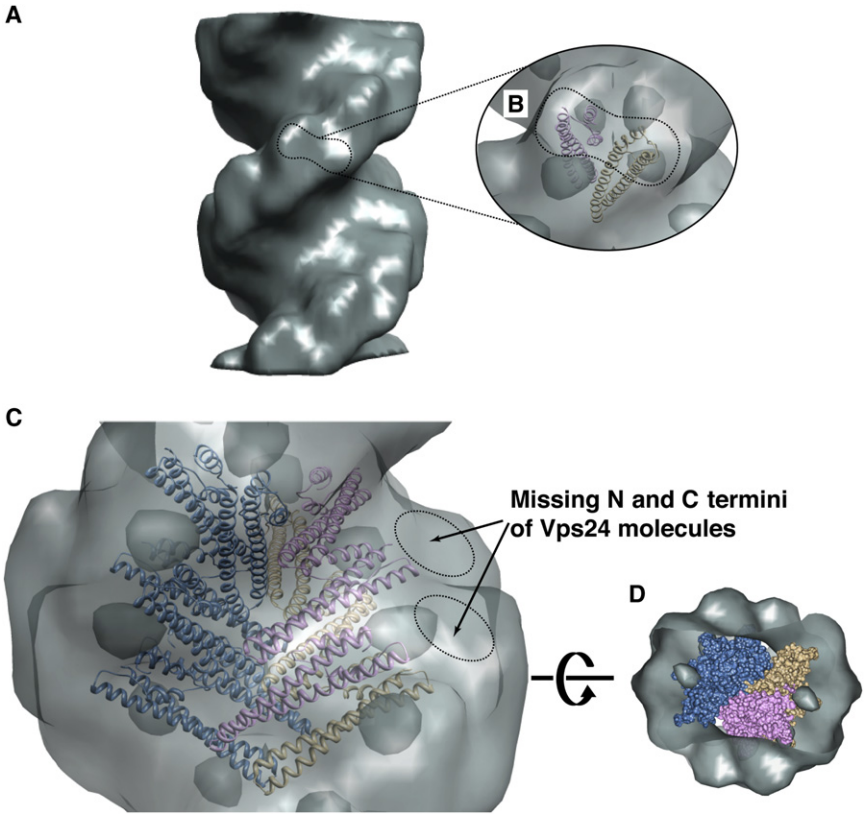

Figure 2. ScVps24 Forms a Two-Stranded Helical Filament

(A) The 3D reconstruction of negatively stained ScVps24 helical filaments shown as a gray surface. The 25 Å resolution reconstruction was generated from single-particle averaging of ~9000 segments that sorted to a pitch of ~260 Å. The knuckles formed by the repeating unit of Vps24 molecules are outlined in black.

(B) The model for the Vps24 subunits (residues 14–140) fitted in the reconstruction, which is shown as a transparent surface. The two molecules within the repeating unit are colored in purple (A molecules) and tan (B molecules).

(C) Side view of the reconstruction. The empty knuckle regions circled in black would be filled by ScVps24 N and C termini that are missing from the Vps24 (CHMP3) crystal structure, which was used as a model for the fitting. One strand is colored all in blue and the other in purple (A molecules) and tan (B molecules), representing the two layers of molecules within a repeating unit.

(D) Axial view of the reconstruction with Vps24 molecules shown in a molecular surface representation. The strands are colored as above.

ScVps24 1–186, lacking the C terminus, is able to form filaments, although they are more disordered and have a reduced diameter (~11 nm) (data not shown). If the crystallographically observed dimer (dimer 1 of Muziol et al., 2006) were present in a radial arrangement, the two-fold symmetry would dictate that one C terminus of the dimer would be at the center of the filament and the other at the periphery, an arrangement that is inconsistent with our observation that the C terminus is not essential for filament formation. If this putative dimer were arranged tangentially to the helix, both C termini could protrude away from the filament. However, such an arrangement would leave a hole down the center of the filaments, which is not consistent with the reconstructed density. There is a region of lower density that can be seen as a pocket roughly halfway between the knuckle and the center of the filament (Figure 2). Avoiding threading protein through this pocket further restricts fitting a dimer into the helical reconstruction. The extreme N terminus of Vps24 (equivalent to residues 1–9 of human Vps24, which is not present in the crystal structure) is also expected to contribute to knuckle density. The repeating unit of the filaments appears to contain two molecules of Vps24 (Figure 2B) and is repeated approximately nine times per turn on each strand, resulting in ~36 molecules per turn of a two-stranded helix.

The Intra- and Interstrand Packing within a Filament

There are two molecules within a repeating unit of each strand in the filament, molecules A and B (Figure 3). These are arranged so that each of the two strands of the filament consists of two layers, an A layer and a B layer. Within the A layer, successive molecules are roughly parallel to each other, with helix α4 of one molecule packing into the interhelical groove of the α1/α2 helical hairpin from an adjacent molecule in the same layer (A/A^{+1} contact in Figure 3B). Within the B layer, successive molecules are also approximately parallel, with helix α4 of one molecule packing against helix α1 of the next molecule (B/B^{+1} contact in Figure 3). In both layers, additional contacts are made between the α3/α4 loop and helix α1 of adjacent molecules. Contacts between layers within a strand involve helices α2 and α3 of the A layer interacting with the B layer α1/α2 loop and helix α1, respectively (Figure 3C). Two types of contacts hold the two strands of the filament together. First, the B molecules from opposite strands contact each other at the center of the filament, with the N-terminal ends of their helices α2 in a head-to-head fashion. These residues in α2 are equivalent to those essential for head-to-head dimerization of human CHMP3 (dimer 2 in Muziol et al., 2006). Second, a molecule from the A layer of one strand uses its α1/α2 loop to contact the middle of helix α2 of a molecule in layer B of the other strand (Figure 3D). There are no contacts between the A layer in one strand and the A layer from the other strand of the filament. All of the contacts in the model of the helical reconstruction are summarized in Figure S2.

Mutations Affecting Filament Formation In Vitro Also Affect Sorting In Vivo

Because of the low resolution of the reconstruction, there is some uncertainty of the molecular interpretation of the filaments, so we carried out site-specific mutagenesis to test the contacts predicted by the model and their biological importance. Helix α4

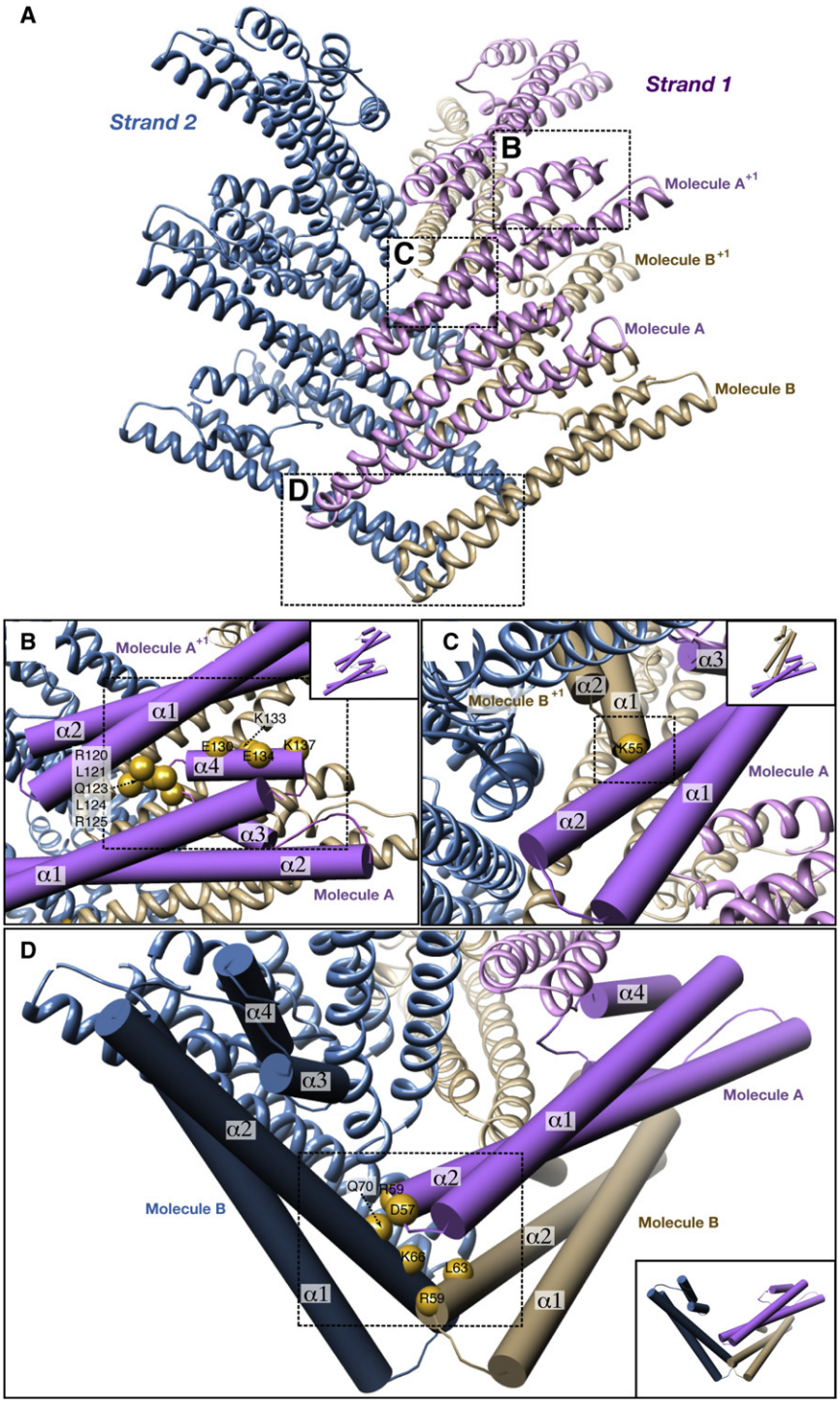

Figure 3. Key Contacts in Filament Formation

(A) The arrangement of Vps24 molecules in the helical filament reconstruction. Strand 1 is shown in purple and tan and strand 2 is shown in blue. The repeating unit in each strand consists of two molecules, which form two layers designated as molecules A (purple) and molecules B (tan). The C termini of both molecules point in the same direction, toward the surface of the filament. The molecules in the repeating unit one symmetry operation above positions A and B are labeled as A^{+1} and B^{+1}, respectively. Close-ups of key interaction areas boxed in black are shown in B–D, where the Cα of residues found to be essential for efficient filament formation are shown as spheres (gold). The insets display schematic representations of these interactions.

(B) The intrastrand contacts between the α3/α4 loop and α4 of a molecule A and α1/α2 of a molecule A^{+1}. Residues R120, L121, Q123, L124, R125, E130, K133, E134, and K137 shown in gold are essential for efficient filament formation.

(C) Interlayer, intrastrand contacts between α2 of molecules in position A and the α1/α2 loop of molecules in position B^{+1}. The K55 residue shown in gold is essential for filament formation.

(D) Interstrand contacts between the tips of the α1/α2 hairpins of two molecules in strand 1 and the tip of α2 of a molecule from strand 2. The residues in gold, D57, R59, L63, K66, and Q70, are essential for filament formation.

(residues 125–138) and the α3/α4 loop (residues 118–124) are central to packing between molecules within a strand (Figure 3B), packing along the α1/α2 hairpin (contacting region 35–45 of helix α1 and region 71–78 of α2). Our mutagenesis data show that the α3/α4 loop and α4 are essential for filament formation (Table 1 and Figure 4). Importantly, circular dichroism spectroscopy indicates that these mutations do not unfold Vps24 (Figure S3). Mutations in the α3/α4 loop and in α4 prevent formation of filaments immediately upon concentration (R120E/L121D, L124D/R125E, K133D/E134A, R120E/L124D/K133D, K133D/E134A/K137D, or L121D/Q123R/R125E/E130R; Table 1). However, for two of these mutants (K133D/E134A and L121D/Q123R/R125E/E130R), filaments eventually form after 4 days of incubation at 4°C (Table 1). The lack of polymeric assembly for these mutations is also evident in an analysis of their behavior in ultracentrifugation (Figure S4). Double mutations in the α3/α4 loop and α4 (K133D/E134A, R120E/L121D, or L124D/R125E) expressed in a ΔScVps24 yeast strain produce cargo-sorting defects, with carboxypeptidase S (CPS) accumulating in class E compartments (Figures 4J–4R). Furthermore, a point mutation of a residue involved in packing between the A and B layers within a strand, K55A in the α1/α2 loop, prevents filament formation in vitro (Table 1). Expression of the K55S mutant in a ΔScVps24 yeast strain leads to CPS-sorting defects (Figures 4D–4F).

Mutation of residues involved in contacts between two strands in a filament (L63D and D57R/R59E/L63D/K66E/Q70R) prevents immediate filament formation (Table 1; Figure S4), but filaments do form after 4 days at 4°C (Table 1). The fact that these

Table 1. Summary of Mutants and Their Effects on In Vitro Filament Formation

Mutation	Location	Immediate Filaments?[a]	Filaments after 3–4 Days at 4°C?[a]
R120E/L121D	Intrastrand contacts (loop α3/α4)	No	No
L124D/R125E	Intrastrand contacts (loop α3/α4 and helix α4)	No	No
R120E/L124D/K133D	Intrastrand contacts (loop α3/α4 and helix α4)	No	No
K133D/E134A/K137D	Intrastrand contacts (helix α4)	No	No
L121D/Q123R/R125E/E130R	Intrastrand contacts (loop α3/α4 and helix α4)	No	Yes
K133D/E134A	Intrastrand contacts (helix α4)	No	Yes
K55A	Interlayer contacts (α1/α2 loop and helix α2)	No	No
L63D	Interstrand contacts (helix α2)	No	Yes
D57R/R59E/L63D/K66E/Q70R	Interstrand contacts (helix α2)	No	Yes
K55S/D57R/L63D	Interlayer and interstrand contacts (α1/α2 loop and helix α2)	No	Yes
Δ1–9	N terminus	No	No
K5D/K6D	N terminus	No	No
Y79R	CHMP3 antiparallel dimerization region	Yes	N/A
K180A	Knuckle region (C terminus)	Yes	N/A
E202A/K203A	Knuckle region (C terminus)	Yes	N/A
Δ187–224	Knuckle region (C terminus)	Yes (smaller-diameter filaments)	N/A

N/A, not applicable.
[a] After purification, all mutant and wild-type proteins were concentrated to 10 mg/ml. Aliquots of the concentrated protein were then diluted to 1 mg/ml to prepare grids for EM analysis. If no filaments were visible in this initial examination, the protein stock was incubated at 4°C for 3–4 days and new EM grids were prepared. Some of the mutants that had no filaments in the initial analysis eventually formed filaments after the extended incubation.

interstrand mutations did not completely abolish filament formation suggests a degree of freedom in the interstrand contacts. This is consistent with the flexibility of the filaments and the presence of multistranded helices. It is likely that ScVps24 molecules are able to flex relative to one another within the constraints of the helix. In vivo, expression of an L63D mutant in a ΔScVps24 strain resulted in CPS-sorting defects (Figures 4G–4I). The crystallographic antiparallel dimer observed for CHMP3 (dimer 1 in Muziol et al., 2006) is not present in our model of the filament reconstruction. Y79, a residue in the CHMP3 antiparallel dimerization interface (Muziol et al., 2006), is also involved in packing within the A layer of filaments, but its mutation (Y79R) did not affect in vitro filament formation (Table 1; Figure S4).

We find that residues in the extreme N terminus (residues 1–9) of ScVps24, specifically Lys5 and Lys6 (Table 1; Figure S4), are essential for filament formation. However, because this region is not present in the CHMP3 crystal structure, we could not model the interactions it forms. Although ScVps24 residues 1–9 are necessary for filament formation, they are not sufficient to confer filament formation, because a chimeric protein consisting of ScVps24 residues 1–9 directly fused to residues 10–222 of human CHMP3 failed to form filaments (data not shown).

ScVps24-ScVps2 Chimeric Filaments Can Be Bundled and Disassembled by the ATPase Vps4

In vivo, the AAA-type ATPase Vps4 disassembles the ESCRT lattice from endosomal membranes in an ATP-dependent fashion (Babst et al., 1998). It has been shown that the N-terminal MIT domain of Vps4 recognizes a (D/E)xxLxxRLxxL(K/R) motif in the C termini of the ESCRT-III proteins Vps2 and Did2 (Obita et al., 2007; Stuchell-Brereton et al., 2007). This interaction recruits the ATPase to the endosomal membrane. However, Vps2 and Did2 do not have the same lattice-forming capabilities in vitro as the Vps24 and Snf7 subunits. In order to investigate the ability of Vps4 to disassemble ESCRT-III lattices in vitro, we designed a chimeric ESCRT-III subunit that could both form lattices and recruit Vps4. The chimera consists of the N-terminal helices α1–α5 of ScVps24 (residues 1–179) and the C-terminal, Vps4-binding region of ScVps2 (residues 181–232; Figure 5A). This chimera forms filaments that are indistinguishable from wild-type ScVps24 filaments (Figure 5B). Vps4 in the presence of ATP was able to disassemble preformed chimeric filaments, as indicated by the absence of filaments upon negative staining and EM (Figures 5C and 5G) but had no effect on wild-type ScVps24 filaments (Figure 5D). In the presence of ADP, Vps4 caused the chimeric filaments to arrange into extensive cables (Figures 5E), presumably consisting of oligomers of Vps4 bound to ScVps24 subunits from multiple filaments. Vps4 with ADP had no effect on wild-type ScVps24 filaments (Figures 5F). The ability of Vps4 to disassemble these chimeric filaments was also examined by sedimentation. At a concentration of 2.5 μM, most of the Vps24-Vps2 chimera readily sediments, suggesting that it is present as large assemblies (Figure 5J). This is unaltered by incubating the chimera with Vps4 and ADP. However, when incubated with Vps4 and ATP, the Vps24-Vps2 chimera redistributes to the supernatant (Figure 5H), consistent with the disassembly inferred from the EM results.

Because Vps4 binds ESCRT-III proteins via its MIT domain, we next tested whether the MIT domain mediates the bundling of

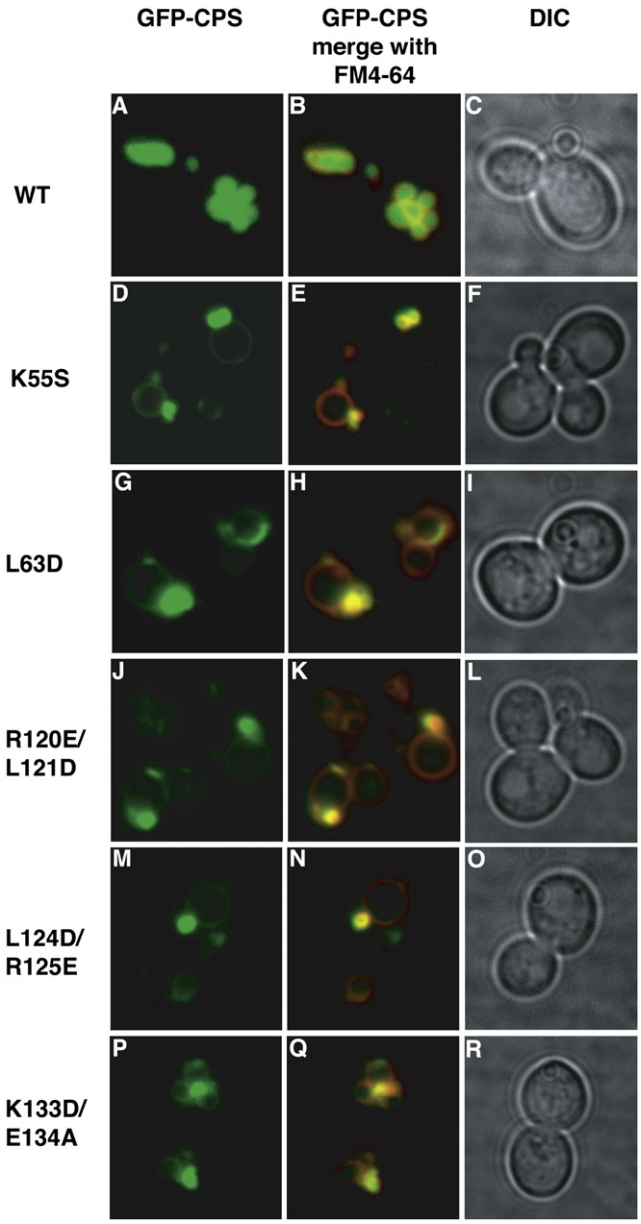

Figure 4. Mutations of Vps24 Residues Important for Filament Formation Cause Cargo Missorting In Vivo

The constructs were examined by fluorescence and differential interference contrast (DIC) microscopy.

(A–C) Yeast cells expressing wild-type Vps24 sort GFP-CPS into vacuoles.

(D–F) Yeast cells transfected with a plasmid expressing Vps24 mutated in K55S, a residue involved in interlayer intrastrand interactions, exhibit a strong GFP-CPS cargo-sorting defect in the context of a *vps24Δ* strain. The MVB cargo protein GFP-CPS accumulates in a class E compartment (membranes labeled by FM4-64). The same phenotype is seen for mutations of residues involved in the following contacts:

(G–I) Interstrand contacts, L63D.

(J–L) Intrastrand contacts at the α3/α4 loop, R120E/L121D.

(M–O) Intrastrand contacts at the α3/α4 loop and α4, L124D/R125E.

(P–R) Intrastrand contacts at α4, K133D/E134A.

chimeric filaments. We found that Vps4 mutated in a residue in helix 3 of the MIT domain, which makes essential contacts with ESCRT-III (L64D; Figure 6), and ΔMIT-Vps4 (data not shown) were unable to either disassemble the chimeric filaments in the presence of ATP or bundle them in the presence of ADP and had no effect on wild-type ScVps24. In order to determine whether the ScVps24-ScVps2 chimera represents a "minimal" unit of the ESCRT-III machinery that can simultaneously form lattices and recruit ScVps4, the chimera was expressed in yeast cells lacking either the Vps2 or Vps24 subunit. The chimeric protein was not able to rescue sorting defects for either of these deletion strains (Figure S5). This suggests that the C terminus of ScVps24 and the N terminus of ScVps2 have important functions in vivo that remain to be characterized.

DISCUSSION

The ESCRT-III subunits exist as soluble monomers in the cytosol and transiently assemble on endosomal membranes to facilitate cargo sorting and ILV formation. For ESCRT-I and –II, the architecture and stoichiometry of the complexes have been characterized. Although numerous biochemical and genetic studies demonstrate specific interactions between the ESCRT-III subunits and suggest that ESCRT-III forms arrays or lattices at endosomal membranes, the stoichiometry and architecture of the ESCRT-III complex is currently unknown.

We have examined the solution behavior of the four recombinant yeast ESCRT-III subunits and found that both Snf7 and Vps24 are able to form self-assemblies in vitro, which we have characterized by negative staining and electron microscopy. Snf7 most readily self-associates, forming sheets (some of which are large enough to be observed by eye), filaments, and rings (Figures 1B–1D). These Snf7 assemblies have proven too disordered for effective structural characterization, suggesting a high degree of flexibility in the contacts between Snf7 subunits. Human Snf7 has recently been shown to form extensive filaments that arrange in circular arrays when overexpressed in COS-7 cells, similar to the yeast Snf7 rings we observe in vitro (Hanson et al., 2008). The second self-associating ESCRT-III subunit, Vps24, forms helical filaments suitable for single-particle EM reconstruction. We have modeled the 25 Å helical reconstruction of a two-stranded ScVps24 filament, using the crystal structure of the core of human Vps24 (CHMP3 9–183; Muziol et al., 2006) (Figure 2). Each strand of the filament consists of two layers (A and B) of Vps24 molecules. Within each layer, molecules are arranged in a roughly parallel fashion. Contacts made by the α4 helix and the α3/α4 loop are prominent in the interactions within the layers. In the A layer, this region packs into the interhelical groove of the α1/α2 hairpin, and in the B layer, it packs against helix α1 of the adjacent molecule (Figure 3 and Figure S2). Interstrand contacts are made largely via the tips of the α1/α2 hairpin, although the variability in pitch that we observe for the two-stranded filaments, together with the presence of higher-order filaments, suggests that both intra- and interstrand contacts are flexible, allowing the angle of molecules with respect to the z axis to vary. Vps24 subunits are highly conserved among orthologs (Muziol et al., 2006), and this conservation is spread over most of the surface of the structural core of Vps24. Most of the residues involved in intermolecular contacts

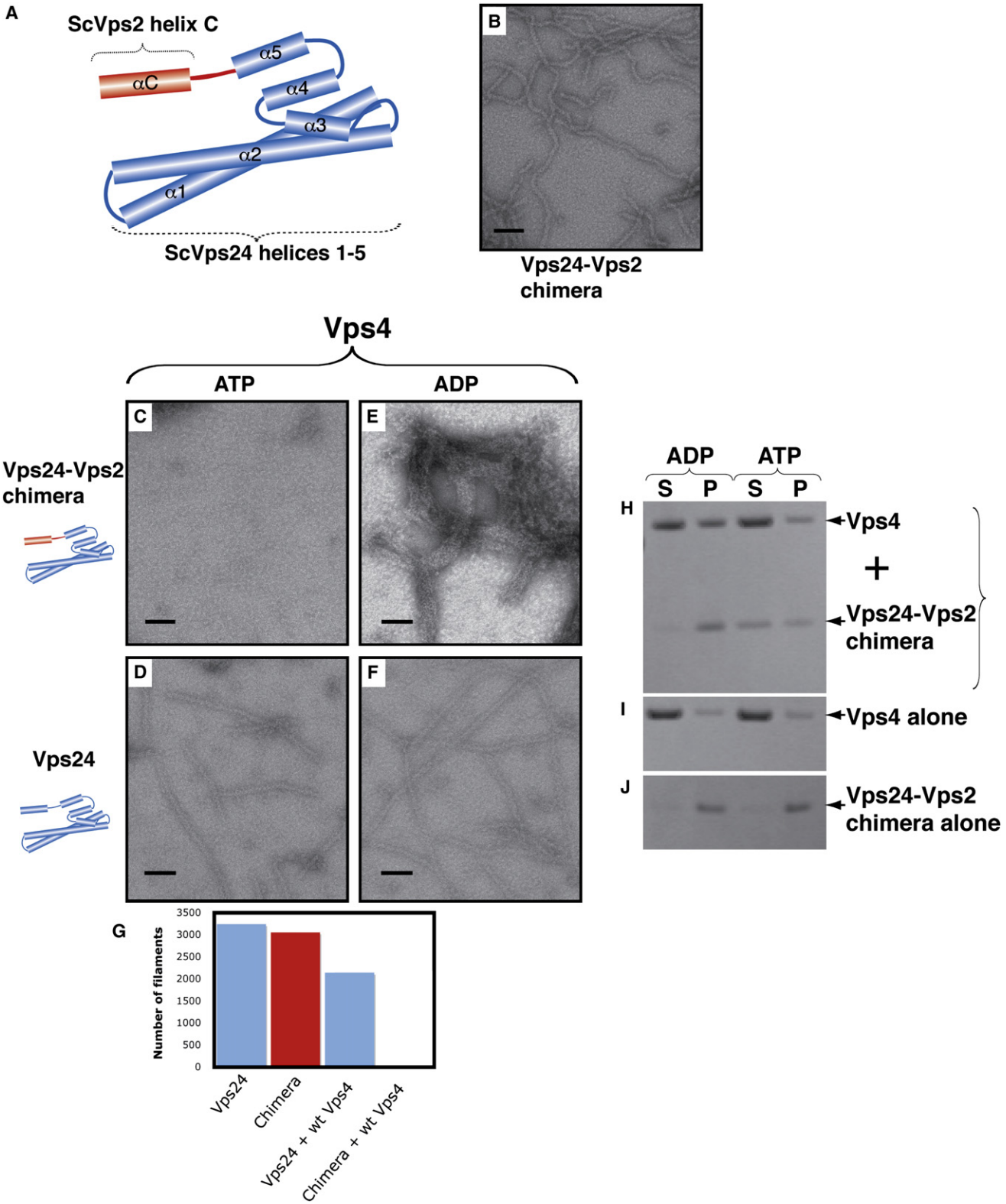

Figure 5. Vps4 Interacts with and Disassembles Vps24-Vps2 Chimeric Filaments

(A) Schematic of Vps24-Vps2 chimera.

(B) Electron micrograph of negatively stained chimeric filaments.

(C and E) Chimeric Vps24-Vps2 filaments in the presence of Vps4, 2 mM $MgSO_4$, and 1 mM ATP (C) or ADP (E).

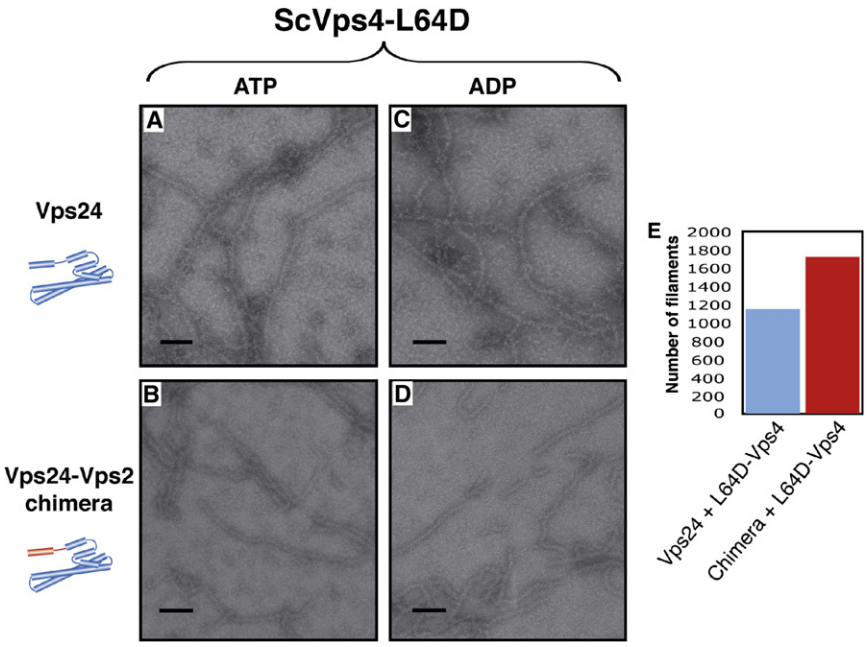

Figure 6. The MIT Domain Is Essential for the Interaction between the Vps24-Vps2 Chimera and Vps4

(A and B) Wild-type Vps24 filaments (A) and chimeric Vps24-Vps2 filaments (B) in the presence of full-length Vps4-L64D mutant and ATP.

(C and D) Wild-type Vps24 filaments (C) and chimeric Vps24-Vps2 filaments (D) with the full-length Vps4-L64D mutant and ADP.

The scale bars represent 100 nm.

(E) Quantitation of the ability of Vps4-L64D to disassemble wild-type Vps24 or chimeric Vps24-Vps2 filaments (prepared as in Figure 5G).

in the model of the helical filaments have a conserved character between Vps24 and Vps2, which is consistent with the suggestion that these subunits assemble as a subcomplex in vivo (Figure S6) (Babst et al., 2002). Residues in key contact areas that are essential for filament formation (Table 1 and Figure 3) are also necessary for efficient cargo sorting in vivo (Figure 4), suggesting that these homopolymeric Vps24 filaments may involve contacts that mimic those present in the ESCRT-III heteropolymers formed in yeast. We cannot exclude that the mutations affect CPS sorting by disrupting interactions of Vps24 with other components of the sorting machinery. However, mutational data suggest a key role for helix α4 and the α3/α4 loop, consistent with in vivo data from human Snf7, which shows that constructs encompassing helices α1–α4 oligomerize more efficiently than helices α1–α3 alone (Shim et al., 2007). In the region corresponding to helix α4, there is a notable difference between the types of residues in Vps24 and Vps2 versus those in Snf7 and Vps20 (Figure S6). This structural element may be a part of the mechanism enabling assembly of Vps2/Vps24 versus Snf7/Vps20 subcomplexes.

The helical filaments observed for Vps24 may be related to the filaments that have been observed in vivo when human Snf7 was overexpressed in COS-7 cells. Similar endogenous filaments (presumably of ESCRT-III components) were observed when an ATP-locked mutant of Vps4 ($VPS4B^{E235Q}$) was overexpressed (Hanson et al., 2008). Both the human Snf7 in vivo and the yeast Snf7 in vitro form ~4–6 nm filaments that are narrower than the ~15 nm yeast Vps24 two-stranded filaments. These Snf7 filaments may represent a single-strand helical filament; however, this is speculative.

Here we have expressed a chimeric ESCRT-III construct capable of simultaneously forming filaments and binding to Vps4. The chimera consists of the α1–α5 helices of ScVps24 (residues 1–179) and the C-terminal, Vps4-binding region of ScVps2 (residues 181–232; Figure 5A). The AAA-ATPase responsible for ESCRT disassembly in yeast, Vps4, was able to disassemble the chimeric assemblies in vitro, in a MIT-domain and ATP-dependent manner. Full-length Vps4 in the presence of ADP was able to bundle the chimeric filaments to form large curved cables of filaments. These bundles presumably consist of Vps4 oligomers simultaneously bound to multiple chimeric filaments and could represent a possible higher-order form of the ESCRT-III array that could exist on membranes, perhaps via interactions between ESCRT-III and MIT-domain-containing accessory proteins (Tsang et al., 2006). Such bundling is also observed in vivo when Snf7 is expressed together with the hydrolysis-deficient $VPS4B^{E235Q}$ (Hanson et al., 2008). Therefore, Vps4 seems able to both bundle and dissociate ESCRT-III polymers. An additional similarity between the Vps24-Vps4 (Figure 5E) and Snf7-Vps4 (Hanson et al., 2008) assemblies is their tendency to form highly curved bundles. Formation of bundles of heteropolymers of ESCRT-III filaments may be an important step toward membrane deformation. Indeed, human Snf7 coexpressed with the hydrolysis-deficient $VPS4B^{E235Q}$ forms buds and tubules that protrude away from the cell surface (Hanson et al., 2008).

In the yeast cytosol, the ESCRT-III subunits exist as soluble monomers, with growing evidence that an internal interaction between their N and C termini holds the monomers in an inactive,

(D and F) Wild-type Vps24 filaments in the presence of Vps4, 2 mM $MgSO_4$, and 1 mM ATP (D) or ADP (F).

The scale bars represent 100 nm.

(G) Quantitation of the ability of Vps4/ATP to disassemble the Vps24 or Vps24-Vps2 chimeric filaments. Fifty images were taken, evenly sampling grids prepared with Vps24 or the Vps24-Vps2 chimera in the presence or absence of Vps4/ATP. The bar graph depicts the total number of filaments found in all of the images for each construct/condition.

(H–J) Sedimentation assay of Vps4-mediated disassembly of Vps24-Vps2 chimera assemblies (H). Chimeric Vps24-Vps2 was incubated with Vps4 and either ADP or ATP, as indicated. The proteins were centrifuged and the pellet (P) and supernatant (S) fractions were analyzed by SDS-PAGE. An InstantBlue (Novexin) stained gel is shown. Individual proteins, Vps4 (I) or Vps24-Vps2 (J), incubated with either ADP or ATP were analyzed in the same manner. Vps4 in the presence of ATP increases the fraction of soluble (nonpolymerized) Vps24-Vps2 chimera (H). Most of the Vps4 was soluble in the presence of ATP, whereas in the presence of ADP more Vps4 was associated with the pellet, presumably bound to polymerized Vps24-Vps2 chimera (H).

autoinhibited state (Shim et al., 2007; Zamborlini et al., 2006; Azmi et al., 2008; Lata et al., 2008). The trigger for release of this inhibition and assembly of the ESCRT-III complex on endosomal membranes is unclear. Protein modifications or interactions with other ESCRT proteins, such as that between Vps20 of ESCRT-III and Vps25 of ESCRT-II, could account for this activation (Teo et al., 2004; Yorikawa et al., 2005), as could interactions with the lipid membrane itself or with unknown protein factors. It is possible that the affinity of the autoinhibitory interaction among the ESCRT-III proteins varies. Our data suggest that two of the ESCRT-III subunits, Snf7 and Vps24, can overcome this autoinhibition and form self-assemblies unaided in vitro, suggesting that they have more lax internal interactions than other ESCRT-IIIs. External factors, such as the high protein concentrations used in this study, may decrease the barrier to self-association, contributing to the formation of the assemblies we observed. The yeast ESCRT-III subunits that do not spontaneously self-associate (Vps20 and Vps2) may be performing different functional roles in the ESCRT-III reaction. Vps20 is required for membrane recruitment of Snf7 (Babst et al., 2002) and thus may ''nucleate'' Snf7 filaments (as proposed in Hurley, 2008). By forming a subcomplex with Vps24 filaments, Vps2 could recruit multiple Vps4(ATP)-Vta1 complexes (both directly and indirectly via ESCRT-III-associated proteins) to the ESCRT-III lattice, facilitating ATP-dependent disassembly (Azmi et al., 2008; Nickerson et al., 2006; Obita et al., 2007; Saksena et al., 2007).

Differences between the autoinhibitory capabilities of ESCRT-III subunits would suggest that the properties and functions of the N and C termini vary among ESCRT-III components. Indeed, the affinity of ESCRT-III C termini for MIT domains has been shown to vary among ESCRT-III subunits (Obita et al., 2007; Stuchell-Brereton et al., 2007; Azmi et al., 2008). Here we have shown that the expression of a chimeric Vps24-Vps2 protein in yeast strains deficient for Vps2 and Vps24 was unable to rescue the GFP-CPS cargo-sorting defect (Figure S5). This suggests that the C terminus of Vps24 and the N terminus of Vps2 have important functions in vivo that remain to be characterized. The data suggest that the properties and functions of the ESCRT-III components are likely to vary greatly among the individual subunits, highlighting the complexity of ESCRT-III autoinhibition and function.

We have shown that Vps24 and Snf7 have the ability to self-assemble in vitro. When equipped with a MIT-interacting motif, the ESCRT-III filaments can be assembled further into large, curved bundles in a MIT-dependent manner that are disassembled only in the presence of Vps4 and ATP. The ability of Vps4 to organize ESCRT-III filaments into curved bundles is unexpected in light of its function in ESCRT disassembly, but might be critical for membrane deformation.

EXPERIMENTAL PROCEDURES

Plasmids

The sequences encoding full-length *Saccharomyces cerevisiae* Vps24 (amino acids 1–224) and Vps2 (amino acids 1–232) were optimized for codon usage in *Escherichia coli*, synthesized (http://www.genscript.com/), and inserted into a pUC57 vector. They were then subcloned into the expression vector pOPTH-tev using NdeI-BamHI sites, resulting in an MAH_6SSGSENLYFQGSH affinity tag with a TEV-cleavage site immediately preceding the Met1 residue. Full-length ScVps4 (amino acids 1–437) and Snf7 (amino acids 1–240) were PCR amplified from genomic DNA and cloned into the pOPTH expression vector, resulting in an N-terminal MAH_6 affinity tag. ScVps24 (1–186) and ScVps24 (10–224) were cloned into the pOPTH-tev vector, and ScVps4 (122–437) into the pOPTG expression vector and expressed with an N-terminal GST tag. Point mutations were generated by overlapping PCR or by using the QuikChange mutagenesis kit (Stratagene). The Vps4 (1–437) L64D mutant was subcloned into the pOPTG vector and expressed with an N-terminal GST tag. The chimeric ScVps24 (1–179)-ScVps2 (181–232) protein was generated using overlapping PCR and cloned into the pOPTH-tev vector. All plasmids were verified by sequencing.

For expression in yeast, ScVps24 (1–224) and ScVps24 (1–179)-ScVps2 (181–232) with the original *S. cerevisiae* codon usage were cloned into the yeast vector pRB415A encoding an N-terminal Myc tag. Vps24::His (Vps24 replaced by the His gene) yeast strains were transformed with ScVps24 (1–224) or with ScVps24 (1–224) point mutants as previously described (Efe et al., 2007) and analyzed by microscopy. All plasmids were verified by sequencing.

Expression and Purification of Proteins

All constructs were expressed in C41 (DE3) cells, grown at 37°C to OD_{600nm} = 1.0, and then induced with 0.3 mM IPTG at 37°C for 3 hr. All His_6-tagged proteins were purified by Ni^{2+}-affinity, heparin-Sepharose, Q-Sepharose, and gel-filtration chromatography. Where a cleavable His_6 tag was used, overnight TEV protease cleavage preceded the Q-Sepharose purification step. Snf7, chimeric Vps24-Vps2, and all Vps24 constructs were gel filtered in buffer A (20 mM Tris [pH 8.0], 100 mM NaCl). For Vps4, the heparin-Sepharose purification step was omitted and the proteins were gel filtered in buffer B (20 mM Tris [pH 7.4], 100 mM NaCl, 2 mM DTT or 2 mM β-mercaptoethanol).

The GST fusion proteins were purified on glutathione-Sepharose 4B (GE Healthcare). The resin was washed with buffer C (20 mM Tris [pH 7.5], 100 mM NaCl, 2 mM β-mercaptoethanol) followed by buffer D (20 mM Tris [pH 7.5], 200 mM NaCl, 2 mM β-mercaptoethanol) and finally buffer C again. Protein was cut from the beads by overnight TEV cleavage and the cut material was subjected to gel filtration in buffer B.

Specimen Preparation and EM Imaging

Copper grids (400 mesh, 3.05 mm; Agar Scientific) were carbon coated as previously described (Bernal and Stock, 2004). For ScVps24 reconstruction, protein samples purified as described were diluted to 1 mg/ml with buffer A and pipetted onto the surface of the carbon grid. After 30 s, the samples were blotted off with filter paper and stained with 2% (w/v) uranyl acetate. Grids were then left to air dry. Images were collected on an EM208 transmission electron microscope (Philips) at a nominal magnification of 40,000×. Images were recorded on Kodak SO-163 film and scanned on a KZA scanner (Henderson et al., 2007) to give a final sampling of 1.25 Å/pixel.

Image Processing and 3D Reconstruction

The BOXER program of the EMAN 1.8 software package (Ludtke et al., 1999) was used to manually select two-stranded filaments from which 85,000 segments were cut as 200 × 400 pixel boxes at 1.25 Å/pixel with a 369 pixel overlap. All images were compressed by averaging adjacent pixels to 5 Å/pixel, and padded to 100 × 100 pixel boxes, followed by a band-pass filter (high-resolution cutoff, 1/[20 Å]; low-resolution cutoff, 1/[250 Å]) and normalization. Variability in pitch was estimated from the axial distance of the layer line with Bessel order 2 on summed power spectra, and a series of smooth helices with pitches that sampled this range (240–350 Å) was generated. The two-stranded data set was sorted against these helices and images from each pitch bin were extracted and treated separately. Power spectra were generated from the separate pitch bins and where possible used to estimate the rise per subunit of the filament segments and therefore the number of subunits per turn. These values were used to run the IHRSR software (Egelman, 2007; Frank et al., 1996) using a solid cylinder as a starting model for bins with mean pitches of 260, 270, 280, 290, 300, and 310 Å. The reconstruction from images in the 260 Å bin was chosen for modeling, on the basis of the number of images it contained and power spectra quality. To try to improve the 260 Å pitch model, the remaining heterogeneity of the data set was addressed. In order to do this, at each iteration, 20% of images with the lowest correlation coefficients were excluded from contributing to the 3D model for the next iteration. However, inclusion of this

step did not significantly affect the appearance or final helical parameters of the model, and the reconstruction from data treated in this way is shown in the figures. After 50 cycles, the analysis showed that in addition to the helical symmetry (rotation of 38.5° degrees and translation of 27.3 Å per subunit), there was also two-fold rotational symmetry. To estimate the resolution of the final reconstruction, the two-stranded data set was split randomly in half and used to generate two independent reconstructions (Yang et al., 2003). The resolution of the reconstruction was estimated as 25 Å using the 0.5 Fourier shell correlation criterion. Visualization of the EM surface envelope was done using the UCSF Chimera package (Pettersen et al., 2004). The atomic model of Vps24 (Protein Data Bank ID code 2GD5; Muziol et al., 2006) was docked by eye into the EM reconstruction of the ScVps24 filament, the shape of which strongly restricts the possible molecular packings. Helical symmetry was applied to the atomic coordinates of a repeating unit to generate the filament model. Inter- and intrastrand contact regions were identified and used to design mutants that were expressed as described.

Microscopy of ScVps24 Mutants

Cells expressing fluorescent fusion proteins were grown in minimal media to OD_{600nm} = 0.5. Cells were stained with FM4-64 as previously described for visualizing the vacuolar membrane or the class E compartment (Vida et al., 1993). Microscopy was performed using a Delta Vision RT microscope (Applied Precision) equipped with FITC and rhodamine filters. Images were captured with a digital camera (Cool Snap HQ, Photometrics).

Sedimentation Analysis of Filament Disassembly

Vps24-Vps2 chimeric filaments were mixed with the Vps4 constructs, 2.5 μM each, in the presence of 0.5 mM ATP or ADP and 0.5 mM $MgCl_2$. Reaction mixtures (30 μl) were incubated at 4°C for 20 min. After ultracentifugation in a TLA100 rotor at 50,000 rpm for 30 min at 10°C, the supernatants were removed and 10 μl of 4× SDS sample buffer was added. Pellets were dissolved in 40 μl 1× SDS sample buffer. Equal volumes of supernatant (S) and pellet (P) fractions were analyzed on a 4%–12% Bis-Tris gel run with MES buffer (Invitrogen). Gels were stained with InstantBlue (Novexin).

EM Analysis of Filament Disassembly

Preformed Vps24 and Vps24-Vps2 chimeric filaments were mixed with the Vps4 constructs in a 2:1 molar ratio, with a final concentration of 20 μM Vps24/chimera. The reactions were performed in the absence or presence of 1 mM ATP or ADP (Sigma; neutralized) and 2 mM $MgSO_4$. Reaction mixtures were incubated at 4°C for 10 min and used to make grids for EM analysis as described. Control reactions of Vps24/chimera with ATP or ADP and $MgSO_4$ and Vps4 protein alone were also carried out. For the quantitation of filament disassembly, 50 images were taken at a nominal magnification of 40,000×, evenly sampling EM grids in a rectilinear pattern with 130 μm intervals.

SUPPLEMENTAL DATA

Supplemental Data include six figures, Supplemental References, and one movie and can be found with this article online at http://www.structure.org/cgi/content/full/16/9/1345/DC1/.

ACKNOWLEDGMENTS

We thank Olga Perisic for invaluable help with cloning, discussions, and advice, Taka Obita for reagents, and Shaoxia Chen and Ricardo Bernal for microscopy advice. Molecular graphics images were produced using the UCSF Chimera package from the Resource for Biocomputing, Visualization, and Informatics at the University of California, San Francisco (supported by NIH grant P41 RR-01081) (Pettersen et al., 2004). S.G.-T. was supported by studentships from Trinity College, Cambridge, and the Medical Research Council. A.V.P. was supported by an EMBO fellowship (ALTF 165-2007). This research was funded by the NIH (E.H.E.) and the Medical Research Council (R.L.W.).

Received: April 1, 2008
Revised: June 15, 2008
Accepted: June 24, 2008
Published: September 9, 2008

REFERENCES

Agromayor, M., and Martin-Serrano, J. (2006). Interaction of AMSH with ESCRT-III and deubiquitination of endosomal cargo. J. Biol. Chem. *281*, 23083–23091.

Azmi, I., Davies, B., Dimaano, C., Payne, J., Eckert, D., Babst, M., and Katzmann, D.J. (2006). Recycling of ESCRTs by the AAA-ATPase Vps4 is regulated by a conserved VSL region in Vta1. J. Cell Biol. *172*, 705–717.

Azmi, I.F., Davies, B.A., Xiao, J., Babst, M., Xu, Z., and Katzmann, D.J. (2008). ESCRT-III family members stimulate Vps4 ATPase activity directly or via Vta1. Dev. Cell *14*, 50–61.

Babst, M., Wendland, B., Estepa, E.J., and Emr, S.D. (1998). The Vps4p AAA ATPase regulates membrane association of a Vps protein complex required for normal endosome function. EMBO J. *17*, 2982–2993.

Babst, M., Katzmann, D.J., Estepa-Sabal, E.J., Meerloo, T., and Emr, S.D. (2002). ESCRT-III: an endosome-associated heterooligomeric protein complex required for MVB sorting. Dev. Cell *3*, 271–282.

Bache, K.G., Stuffers, S., Malerod, L., Slagsvold, T., Raiborg, C., Lechardeur, D., Walchli, S., Lukacs, G.L., Brech, A., and Stenmark, H. (2006). The ESCRT-III subunit hVps24 is required for degradation but not silencing of the epidermal growth factor receptor. Mol. Biol. Cell *17*, 2513–2523.

Bernal, R.A., and Stock, D. (2004). Three-dimensional structure of the intact *Thermus thermophilus* H^+-ATPase/synthase by electron microscopy. Structure *12*, 1789–1798.

Bowers, K., Lottridge, J., Helliwell, S.B., Goldthwaite, L.M., Luzio, J.P., and Stevens, T.H. (2004). Protein-protein interactions of ESCRT complexes in the yeast *Saccharomyces cerevisiae*. Traffic *5*, 194–210.

Carlton, J.G., and Martin-Serrano, J. (2007). Parallels between cytokinesis and retroviral budding: a role for the ESCRT machinery. Science *316*, 1908–1912.

DeRosier, D.J., and Klug, A. (1968). Reconstruction of three dimensional structures from electron micrographs. Nature *217*, 130–134.

Doyotte, A., Russell, M.R., Hopkins, C.R., and Woodman, P.G. (2005). Depletion of TSG101 forms a mammalian "class E" compartment: a multicisternal early endosome with multiple sorting defects. J. Cell Sci. *118*, 3003–3017.

Efe, J.A., Botelho, R.J., and Emr, S.D. (2007). Atg18 regulates organelle morphology and Fab1 kinase activity independent of its membrane recruitment by phosphatidylinositol 3,5-bisphosphate. Mol. Biol. Cell *18*, 4232–4244.

Egelman, E.H. (2000). A robust algorithm for the reconstruction of helical filaments using single-particle methods. Ultramicroscopy *85*, 225–234.

Egelman, E.H. (2007). The iterative helical real space reconstruction method: surmounting the problems posed by real polymers. J. Struct. Biol. *157*, 83–94.

Filimonenko, M., Stuffers, S., Raiborg, C., Yamamoto, A., Malerod, L., Fisher, E.M., Isaacs, A., Brech, A., Stenmark, H., and Simonsen, A. (2007). Functional multivesicular bodies are required for autophagic clearance of protein aggregates associated with neurodegenerative disease. J. Cell Biol. *179*, 485–500.

Forman, M.S., Trojanowski, J.Q., and Lee, V.M. (2004). Neurodegenerative diseases: a decade of discoveries paves the way for therapeutic breakthroughs. Nat. Med. *10*, 1055–1063.

Frank, J., Radermacher, M., Penczek, P., Zhu, J., Li, Y., Ladjadj, M., and Leith, A. (1996). SPIDER and WEB: processing and visualization of images in 3D electron microscopy and related fields. J. Struct. Biol. *116*, 190–199.

Fujita, H., Umezuki, Y., Imamura, K., Ishikawa, D., Uchimura, S., Nara, A., Yoshimori, T., Hayashizaki, Y., Kawai, J., Ishidoh, K., et al. (2004). Mammalian class E Vps proteins, SBP1 and mVps2/CHMP2A, interact with and regulate the function of an AAA-ATPase SKD1/Vps4B. J. Cell Sci. *117*, 2997–3009.

Haigler, H.T., McKanna, J.A., and Cohen, S. (1979). Direct visualization of the binding and internalization of a ferritin conjugate of epidermal growth factor in human carcinoma cells A-431. J. Cell Biol. *81*, 382–395.

Hanson, P.I., Roth, R., Lin, Y., and Heuser, J.E. (2008). Plasma membrane deformation by circular arrays of ESCRT-III protein filaments. J. Cell Biol. *180*, 389–402.

Hartmann, C., Chami, M., Zachariae, U., de Groot, B.L., Engel, A., and Grutter, M.G. (2008). Vacuolar protein sorting: two different functional states of the AAA-ATPase Vps4p. J. Mol. Biol. *377*, 352–363.

Henderson, R., Cattermole, D., McMullan, G., Scotcher, S., Fordham, M., Amos, W.B., and Faruqi, A.R. (2007). Digitisation of electron microscope films: six useful tests applied to three film scanners. Ultramicroscopy *107*, 73–80.

Hurley, J.H. (2008). ESCRT complexes and the biogenesis of multivesicular bodies. Curr. Opin. Cell Biol. *20*, 4–11.

Katzmann, D.J., Babst, M., and Emr, S.D. (2001). Ubiquitin-dependent sorting into the multivesicular body pathway requires the function of a conserved endosomal protein sorting complex, ESCRT-I. Cell *106*, 145–155.

Katzmann, D.J., Odorizzi, G., and Emr, S.D. (2002). Receptor downregulation and multivesicular-body sorting. Nat. Rev. Mol. Cell Biol. *3*, 893–905.

Kim, J., Sitaraman, S., Hierro, A., Beach, B.M., Odorizzi, G., and Hurley, J.H. (2005). Structural basis for endosomal targeting by the Bro1 domain. Dev. Cell *8*, 937–947.

Lata, S., Roessle, M., Solomons, J., Jamin, M., Gottlinger, H.G., Svergun, D.I., and Weissenhorn, W. (2008). Structural basis for autoinhibition of ESCRT-III CHMP3. J. Mol. Biol. *378*, 816–825.

Lee, J.A., Beigneux, A., Ahmad, S.T., Young, S.G., and Gao, F.B. (2007). ESCRT-III dysfunction causes autophagosome accumulation and neurodegeneration. Curr. Biol. *17*, 1561–1567.

Lin, Y., Kimpler, L.A., Naismith, T.V., Lauer, J.M., and Hanson, P.I. (2005). Interaction of the mammalian endosomal sorting complex required for transport (ESCRT) III protein hSnf7-1 with itself, membranes, and the AAA^+ ATPase SKD1. J. Biol. Chem. *280*, 12799–12809.

Lloyd, T.E., Atkinson, R., Wu, M.N., Zhou, Y., Pennetta, G., and Bellen, H.J. (2002). Hrs regulates endosome membrane invagination and tyrosine kinase receptor signaling in *Drosophila*. Cell *108*, 261–269.

Lottridge, J.M., Flannery, A.R., Vincelli, J.L., and Stevens, T.H. (2006). Vta1p and Vps46p regulate the membrane association and ATPase activity of Vps4p at the yeast multivesicular body. Proc. Natl. Acad. Sci. USA *103*, 6202–6207.

Ludtke, S.J., Baldwin, P.R., and Chiu, W. (1999). EMAN: semiautomated software for high-resolution single-particle reconstructions. J. Struct. Biol. *128*, 82–97.

Martin-Serrano, J., Yarovoy, A., Perez-Caballero, D., and Bieniasz, P.D. (2003). Divergent retroviral late-budding domains recruit vacuolar protein sorting factors by using alternative adaptor proteins. Proc. Natl. Acad. Sci. USA *100*, 12414–12419.

Morita, E., Sandrin, V., Chung, H.Y., Morham, S.G., Gygi, S.P., Rodesch, C.K., and Sundquist, W.I. (2007). Human ESCRT and ALIX proteins interact with proteins of the midbody and function in cytokinesis. EMBO J. *26*, 4215–4227.

Muziol, T., Pineda-Molina, E., Ravelli, R.B., Zamborlini, A., Usami, Y., Gottlinger, H., and Weissenhorn, W. (2006). Structural basis for budding by the ESCRT-III factor CHMP3. Dev. Cell *10*, 821–830.

Nickerson, D.P., West, M., and Odorizzi, G. (2006). Did2 coordinates Vps4-mediated dissociation of ESCRT-III from endosomes. J. Cell Biol. *175*, 715–720.

Obita, T., Saksena, S., Ghazi-Tabatabai, S., Gill, D.J., Perisic, O., Emr, S.D., and Williams, R.L. (2007). Structural basis for selective recognition of ESCRT-III by the AAA ATPase Vps4. Nature *449*, 735–739.

Odorizzi, G., Babst, M., and Emr, S.D. (1998). Fab1p PtdIns(3)P 5-kinase function essential for protein sorting in the multivesicular body. Cell *95*, 847–858.

Pettersen, E.F., Goddard, T.D., Huang, C.C., Couch, G.S., Greenblatt, D.M., Meng, E.C., and Ferrin, T.E. (2004). UCSF Chimera—a visualization system for exploratory research and analysis. J. Comput. Chem. *25*, 1605–1612.

Piper, R.C., and Luzio, J.P. (2007). Ubiquitin-dependent sorting of integral membrane proteins for degradation in lysosomes. Curr. Opin. Cell Biol. *19*, 459–465.

Raymond, C.K., Howald-Stevenson, I., Vater, C.A., and Stevens, T.H. (1992). Morphological classification of the yeast vacuolar protein sorting mutants: evidence for a prevacuolar compartment in class E vps mutants. Mol. Biol. Cell *3*, 1389–1402.

Razi, M., and Futter, C.E. (2006). Distinct roles for Tsg101 and Hrs in multivesicular body formation and inward vesiculation. Mol. Biol. Cell *17*, 3469–3483.

Rieder, S.E., Banta, L.M., Kohrer, K., McCaffery, J.M., and Emr, S.D. (1996). Multilamellar endosome-like compartment accumulates in the yeast vps28 vacuolar protein sorting mutant. Mol. Biol. Cell *7*, 985–999.

Row, P.E., Liu, H., Hayes, S., Welchman, R., Charalabous, P., Hofmann, K., Clague, M.J., Sanderson, C.M., and Urbe, S. (2007). The MIT domain of UBPY constitutes a CHMP binding and endosomal localization signal required for efficient epidermal growth factor receptor degradation. J. Biol. Chem. *282*, 30929–30937.

Saksena, S., Sun, J., Chu, T., and Emr, S.D. (2007). ESCRTing proteins in the endocytic pathway. Trends Biochem. Sci. *32*, 561–573.

Scott, A., Chung, H.Y., Gonciarz-Swiatek, M., Hill, G.C., Whitby, F.G., Gaspar, J., Holton, J.M., Viswanathan, R., Ghaffarian, S., Hill, C.P., and Sundquist, W.I. (2005). Structural and mechanistic studies of VPS4 proteins. EMBO J. *24*, 3658–3669.

Shim, J.H., Xiao, C., Hayden, M.S., Lee, K.Y., Trombetta, E.S., Pypaert, M., Nara, A., Yoshimori, T., Wilm, B., Erdjument-Bromage, H., et al. (2006). CHMP5 is essential for late endosome function and down-regulation of receptor signaling during mouse embryogenesis. J. Cell Biol. *172*, 1045–1056.

Shim, S., Kimpler, L.A., and Hanson, P.I. (2007). Structure/function analysis of four core ESCRT-III proteins reveals common regulatory role for extreme C-terminal domain. Traffic *8*, 1068–1079.

Slagsvold, T., Pattni, K., Malerod, L., and Stenmark, H. (2006). Endosomal and non-endosomal functions of ESCRT proteins. Trends Cell Biol. *16*, 317–326.

Stuchell-Brereton, M.D., Skalicky, J.J., Kieffer, C., Karren, M.A., Ghaffarian, S., and Sundquist, W.I. (2007). ESCRT-III recognition by VPS4 ATPases. Nature *449*, 740–744.

Teo, H., Perisic, O., Gonzalez, B., and Williams, R.L. (2004). ESCRT-II, an endosome-associated complex required for protein sorting: crystal structure and interactions with ESCRT-III and membranes. Dev. Cell *7*, 559–569.

Tsang, H.T., Connell, J.W., Brown, S.E., Thompson, A., Reid, E., and Sanderson, C.M. (2006). A systematic analysis of human CHMP protein interactions: additional MIT domain-containing proteins bind to multiple components of the human ESCRT III complex. Genomics *88*, 333–346.

Vajjhala, P.R., Catchpoole, E., Nguyen, C.H., Kistler, C., and Munn, A.L. (2007). Vps4 regulates a subset of protein interactions at the multivesicular endosome. FEBS J. *274*, 1894–1907.

Vida, T.A., Huyer, G., and Emr, S.D. (1993). Yeast vacuolar proenzymes are sorted in the late Golgi complex and transported to the vacuole via a prevacuolar endosome-like compartment. J. Cell Biol. *121*, 1245–1256.

von Schwedler, U.K., Stuchell, M., Muller, B., Ward, D.M., Chung, H.Y., Morita, E., Wang, H.E., Davis, T., He, G.P., Cimbora, D.M., et al. (2003). The protein network of HIV budding. Cell *114*, 701–713.

Ward, D.M., Vaughn, M.B., Shiflett, S.L., White, P.L., Pollock, A.L., Hill, J., Schnegelberger, R., Sundquist, W.I., and Kaplan, J. (2005). The role of LIP5 and CHMP5 in multivesicular body formation and HIV-1 budding in mammalian cells. J. Biol. Chem. *280*, 10548–10555.

Williams, R.L., and Urbe, S. (2007). The emerging shape of the ESCRT machinery. Nat. Rev. Mol. Cell Biol. *8*, 355–368.

Xiao, J., Xia, H., Zhou, J., Azmi, I.F., Davies, B.A., Katzmann, D.J., and Xu, Z. (2008). Structural basis of vta1 function in the multivesicular body sorting pathway. Dev. Cell *14*, 37–49.

Yang, S., Yu, X., Galkin, V.E., and Egelman, E.H. (2003). Issues of resolution and polymorphism in single-particle reconstruction. J. Struct. Biol. *144*, 162–171.

Yorikawa, C., Shibata, H., Waguri, S., Hatta, K., Horii, M., Katoh, K., Kobayashi, T., Uchiyama, Y., and Maki, M. (2005). Human CHMP6, a myristoylated ESCRT-III protein, interacts directly with an ESCRT-II component EAP20 and regulates endosomal cargo sorting. Biochem. J. *387*, 17–26.

Yu, Z., Gonciarz, M.D., Sundquist, W.I., Hill, C.P., and Jensen, G.J. (2008). Cryo-EM structure of dodecameric Vps4p and its 2:1 complex with Vta1p. J. Mol. Biol. *377*, 364–377.

Zamborlini, A., Usami, Y., Radoshitzky, S.R., Popova, E., Palu, G., and Gottlinger, H. (2006). Release of autoinhibition converts ESCRT-III components into potent inhibitors of HIV-1 budding. Proc. Natl. Acad. Sci. USA *103*, 19140–19145.

